4th Micro and Nano Flows Conference
UCL, London, UK, 7-10 September 2014

Transport properties and structure of fluids in hydrophobic/hydrophilic nanochannels

Filippos SOFOS, Theodoros E. KARAKASIDIS*, Antonios E. GIANNAKOPOULOS, and Antonios LIAKOPOULOS

* Corresponding author: Tel.: +302421074163; Fax: +302421074169; Email: thkarak @uth.gr
Department of Civil Engineering, School of Engineering, University of Thessaly, Volos, GR

Abstract When downsizing towards the nanoscale, system dimensions have been found to affect channel flows mainly because of the presence of the walls that interact strongly with fluid particles. Parameters which are not taken into account at the classical theory continuum theory at the macroscale, should be taken into account at the nano or even micro-scale where the surface to volume ratio increases significantly. Such property is the wall/fluid interaction which determines the wetting (hydrophilic behavior) or not (hydrophobic behavior) of a surface. We first investigate the effect of wall/fluid interaction on fluid atom distribution near the wall through the radial distribution function and, next, we calculate the three most important fluid transport properties, i.e., the diffusion coefficient, shear viscosity and thermal conductivity. Transport properties seem to be affected significantly in the channel region adjacent to the wall.

Keywords: Nano flows, Diffusion Coefficient, Shear Viscosity, Wettability, Radial Distribution Function

1. Introduction

During the past decades, terms like super-hydrophobic surfaces have been incorporated in order to describe hydrophobic surfaces, those where the contact angle between the fluid and the surface is greater than 150^o (Tsai et al. 2009). Apart from experimental techniques employed to study this phenomenon (Baudry et al. 2001; Sedmik et al. 2013), simulation methods such as Molecular Dynamics (MD) or extensions to continuum methods have been widely incorporated and have become a reliable means of providing fundamental guidance to researchers (Vinogradova and Belyaev 2011; Priezjev et al. 2005; Yen 2013). Both experimental and theoretical approaches have revealed that in channel flows past a micro- or nano-channel with hydrophobic walls, due to the reduction in the surface contact area between the flowing liquid and the solid wall, dramatic decrease in the overall flow resistance was observed (Neto et al. 2005). The breakdown of the no-slip hypothesis at the macroscale has been widely investigated at the nanoscale (Asproulis and Drikakis 2010; Yang et al. 2006; Zhang et al. 2012)).

Among other quantities, the calculation of transport properties of fluids such as diffusion coefficient, shear viscosity and thermal conductivity, are of particular interest to investigate as they reveal the mechanisms of energy, heat and mass transfer (Sofos et al. 2009). Atomistic simulation methods can be employed in order to estimate transport properties, although in some cases significant computational cost may be required. However, since experiments are difficult to perform especially at the nanoscale simulation methods constitute the only alternative. In the present work, we perform MD simulations to investigate the structure and transport properties of a fluid past hydrophilic/hydrophobic nanochannel wall. Diffusion coefficient is obtained directly from MD simulations while shear viscosity and thermal conductivity are obtained using the methodology introduced by Giannakopoulos et al. (2012).

2. Molecular Dynamics and Calculations

2.1 Channel model

MD simulations are performed for flat-wall nanochannels, which correspond to macroscopic Poiseuille flow. The system is periodic along the x- and y- directions, while the distance between the two plates is h=6.3nm. The channel modeled is shown schematically in Fig. 1. We divided the

channel flow region in 9 layers along *x*-direction, each one of height h_l=0.7nm, in order to calculate or local structure and transport properties, especially at the vicinity of the wall which is mostly affected by wall interaction.

Atomic interactions between fluid particles are described by Lennard-Jones 12-6 type potentials $u^{LJ}(r_{ij})=4\varepsilon((\sigma / r_{ij})^{12}-(\sigma / r_{ij})^{6}$, where σ is the molecular diameter and ε the energy parameter. Parameters of the LJ potential for Ar are $\sigma_{Ar\text{-}Ar}$ = 3.405 Å and $\varepsilon_{Ar\text{-}Ar}/k_B$= 119.8 K**.** The cut-off frequency above which interatomic interactions are considered zero is $r_c=2.5\sigma_{Ar\text{-}Ar}$.

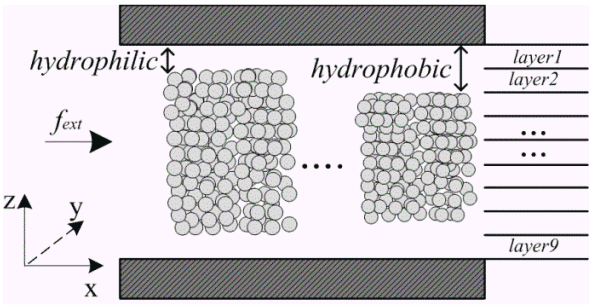

Fig. 1: Schematic representation of the model channel

An external force F_{ext} is applied to the *x*-direction on every fluid particle to drive the flow. Wall atoms are kept bound around their original fcc lattice positions by an elastic string force $\mathbf{F}=-K(\mathbf{r}(t)-r_{eq})$, where $\mathbf{r}(t)$ is the position vector of an atom at time t, r_{eq} is its initial lattice position vector and *K* is the spring constant. This choice of *K* has also been used in previous work (Sofos et al. 2009) and found to satisfy the Lindemann criterion for melting and does not result in oscillating motion of wall particles being outside the regime that can be addressed in the molecular simulation time step.

Wall atoms absorb the increase in kinetic energy of the fluid atoms, which is caused by the application of the external force, and Nose-Hoover thermostats are applied at the thermal walls in order to keep the system's temperature constant (Sofos et al. 2009). We employ two independent thermostats one for the upper wall and another for the lower wall in order to achieve better thermalisation of the wall atoms

A qualitative wall wettability parameter representing hydrophobic or hydrophilic behavior is $\varepsilon_w/\varepsilon_f$ (*w*: wall, *f*: fluid). There is an analogy between this ratio and the fluid contact angle. Following the observations in Voronov et al. (2006) that the contact angle increases with smaller $\varepsilon_w/\varepsilon_f$ and decreases as $\varepsilon_w/\varepsilon_f$ increases, in this work, we investigate wall wettability effect on the flow, for $\varepsilon_w/\varepsilon_f$ values in the range 0.2 – 5.0, covering contact angles from 50° (hydrophobic) to nearly 0° (totally wetting surface).

The simulation step is $\Delta t=10^{-2}$ps. Simulation begins with fluid atoms given appropriate initial velocities in order to reach the desired temperature (*T*=120K). The system reaches equilibrium after an equilibrium run of $2\text{x}10^6$ time steps. Then, a number of NEMD simulations for each channel type are performed, each with duration of $5\text{x}10^5$ time steps.

2.2 Radial Distribution Function

Wall wettability effect is at first explored through the investigation of the radial distribution function *g*(*r*), which presents the distribution of fluid atoms inside the channel, given by

$$g(r)=\frac{\sum_{i=1}^{N}\rho_i(r,z)}{N\overline{\rho(z)}} \qquad (1)$$

where *r* is the radial distance that defines the region of interaction for the i^{th}-particle. We distinct calculations for studying *g*(*r*) between a wall atom and all neighboring fluid atoms inside *r*, $g^{wf}(r)$, and between a fluid atom and all neighboring fluid atoms inside *r*, $g^{ff}(r)$ (Fig. 2).

We calculate the local $g_{lay}(r)$ for each layer as

$$g_{lay}(r)=\frac{\sum_{i=1}^{N_{lay}}\rho_i(r,z)}{N_{lay}\overline{\rho(z)}} \qquad (2)$$

where N_{lay} the number of fluid atoms in the channel layer investigated.

2.3 Transport Properties

The average diffusion coefficient throughout the channel is obtained by particles' trajectories during the simulations from the Einstein's relation

$$\mathrm{D_{ch}} = \lim_{t\to\infty} \frac{1}{2dNt} \left\langle \sum_{j=1}^{N} \left[\mathbf{r}_j(t) - \mathbf{r}_j(0)\right]^2 \right\rangle \qquad (3)$$

where $\mathbf{r}_j$ is the position vector of the j^{th} atom and d is the dimensionality of the system (d=1 for diffusivity calculation in one direction, d=2 in two directions and d=3 in three directions).

For diffusion coefficient calculation in fluid layers parallel to the wall (as shown in Fig. 1), Eq. (3) takes the form

$$\mathrm{D_{lay}} = \lim_{t\to\infty} \frac{1}{2dN_{lay}t} \left\langle \sum_{j=1}^{N} \left[\mathbf{r}_j(t) - \mathbf{r}_j(0)\right]^2 \right\rangle \qquad (4)$$

where N_{lay}: fluid atoms inside the layer under investigation.

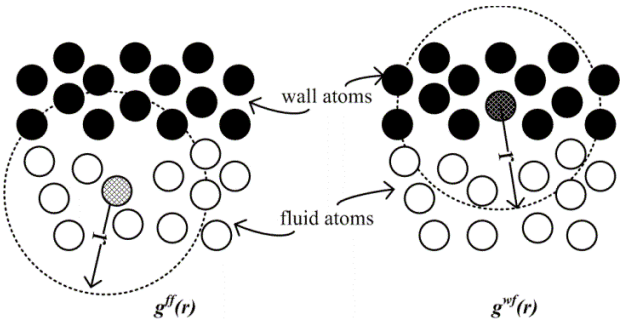

Fig. 2: Distinction between $g^{ff}(r)$ and $g^{wf}(r)$

Atomistic simulation methods usually employ the Green-Kubo formalism to calculate shear viscosity and thermal conductivity for systems at or close to equilibrium, and NEMD methods, which take into account the induced strain rates in a confined channel (Sofos et al. 2010). However, we have to point out that there is extra computational cost for the calculation of these two properties when employing such as scheme.

Giannakopoulos et al. (2012) proposed a linking scheme that connects the three aforementioned transport properties of fluids. The values of the diffusion coefficient, obtained from MD, can be incorporated in classical fluid dynamics relations (Stokes-Einstein) from which we obtain shear viscosity $\eta_{s,ch}$ *and* $\eta_{s,lay}$ using the Stokes-Einstein relation

$$\eta_{s,ch} = \frac{k_B T}{6\pi\sigma \mathrm{D_{ch}}} \qquad (5)$$

$$\eta_{s,lay} = \frac{k_B T}{6\pi\sigma \mathrm{D_{lay}}} \qquad (6)$$

The Stokes-Einstein relation is a good estimate for channels of height $h < 20\sigma$. For thermal conductivity, Giannakopoulos et al. (2012) proposed the relation

$$\lambda_{ch} = \alpha C_v \left(\rho D_{ch} \eta_{s,ch}\right)^{1/2} \qquad (7)$$

and, in the same manner, we have λ_{lay}

$$\lambda_{lay} = \alpha C_v \left(\rho D_{lay} \eta_{s,lay}\right)^{1/2} \qquad (8)$$

where, for argon at 120K, the specific heat is $\mathrm{C}_v = 0.523 \frac{\mathrm{kJ}}{\mathrm{kg\ K}}$, the density considered in the simulations is $\rho = 1078 \frac{\mathrm{kg}}{\mathrm{m}^3}$ and the constant $a \approx 5\times10^6$.

3. Simulation Results

3.1 Fluid structure

We calculate local $g^{ff}(r)$ in channel layers, i.e., $g^{ff}_{lay}(r)$, representing fluid atom distribution inside a channel layer due to neighboring fluid atom interactions. Starting from a highly hydrophobic wall $\left(\varepsilon_w/\varepsilon_f = 0.2\right)$, in Fig. 3(a), we observe that there is small fluid atom localization at layer1, the layer adjacent to the wall, a result we expect since the wall is hydrophobic. As we move on to layer2, 3 and 4, we observe that the fluid atom presence

increases and $g_{lay}^{ff}(r)$ presents its highest peak value for layer 4. As wall hydrophobicity decreases, (Figs. 3(b-d)), there is no significant difference in fluid atom distribution in layers 2, 3 and 4, but layer1 still presents reduced atom distribution.

In Figs. 4(a-d) we present $g_{lay}^{ff}(r)$ in every layer. Figure 4(a) shows how the ratio $\varepsilon_w/\varepsilon_f$ affects distribution in layer 1. For $\varepsilon_w/\varepsilon_f$ =0.2, the $g_{lay}^{ff}(r)$ peak is located at the left of the diagram and moves slightly to the right as the ratio $\varepsilon_w/\varepsilon_f$ increases. Moreover, $g_{lay}^{ff}(r)$ stabilizes to lower value as the wall becomes more hydrophilic. Figures 4(b-d) have almost similar peak value for $g_{lay}^{ff}(r)$, and we observe that at layer 4, in Fig. 4(d), wall interaction does not affect the fluid behavior, since $g_{lay}^{ff}(r)$ is the same for all $\varepsilon_w/\varepsilon_f$ studied.

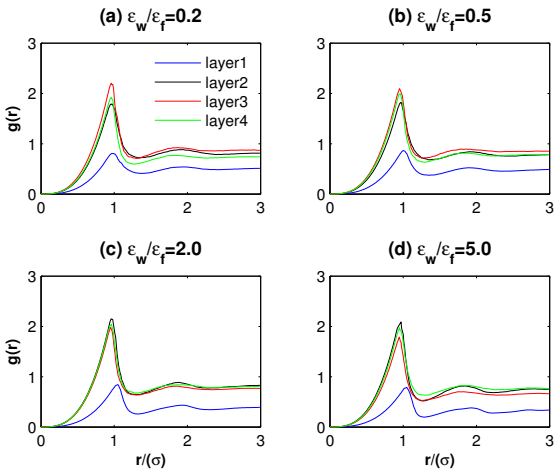

Fig. 3: Local Radial Distribution functions $g_{lay}^{ff}(r)$, from the first 4 channel layers near the wall, for various $\varepsilon_w/\varepsilon_f$ ratios.

Wall particles interact strongly with fluid atoms located at channel layer 1. We remind that, from the Lennard-Jones model we use, the cut-off frequency above which interatomic interactions are considered zero is r_c=2.5σ≈0.85nm and layer 1 width is about 0.7nm. Figure 5 displays fluid atom distribution due to wall interaction in the first channel layer. The peaks values are higher now compared to $g_{lay}^{ff}(r)$.

For $\varepsilon_w/\varepsilon_f$ =0.2, $g_{lay}^{wf}(r)$ is located closer to the wall (at the left), while, as hydrophobicity decreases, $g_{lay}^{wf}(r)$ is moving to the right, away from the wall. The most hydrophilic case, $\varepsilon_w/\varepsilon_f$ =5.0, presents stronger fluid ordering, with a difference between its maximum and minimum $g_{lay}^{wf}(r)$ value at about 70% and 55% between the maximum and the bulk value (where it stabilizes). The respective percentages for the hydrophobic channel $\varepsilon_w/\varepsilon_f$ =0.2 are about 50% and 30%, respectively.

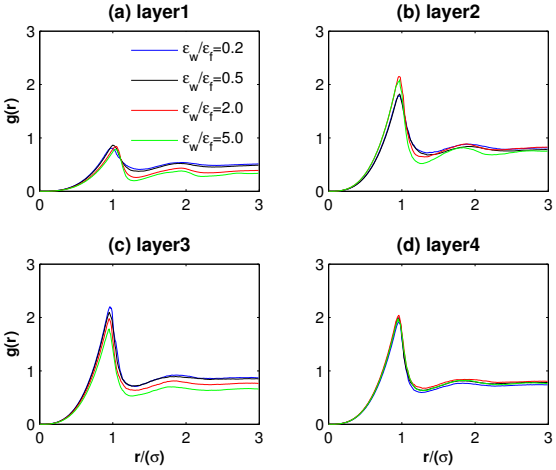

Fig. 4: Local Radial Distribution functions $g_{lay}^{ff}(r)$ for various $\varepsilon_w/\varepsilon_f$ ratios, for the first 4 channel near the wall.

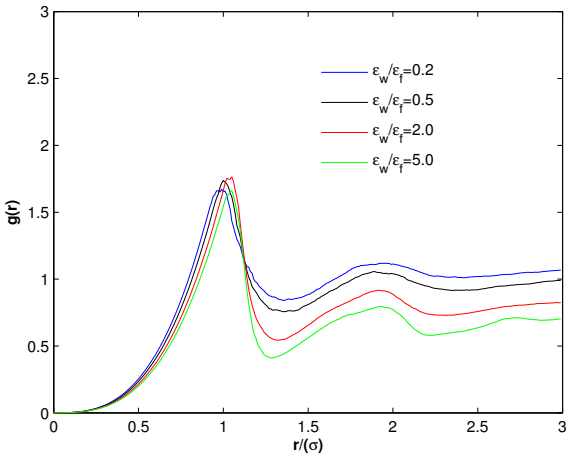

Fig. 5: Local Radial Distribution $g_{lay}^{wf}(r)$ functions for various $\varepsilon_w/\varepsilon_f$ ratios, at layer 1.

3.2 Calculated Transport Properties

We calculate diffusion coefficient, shear viscosity and thermal conductivity as a function of the channel width, as total average channel values from Eqs. (3), (5) and (7), respectively, so as to obtain a qualitative behavior against wall wettability. Equations (5) and (7) are derived from the unified description of Giannakopoulos et al. (2012). For comparison we present also results of transport properties calculated using the Green-Kubo formalism and NEMD methods from Sofos et al. (2009) and Sofos et al. (2010), for the case corresponding to $\varepsilon_w/\varepsilon_f$ =1.2.

Figure 6 presents all transport properties values as a function of the $\varepsilon_w/\varepsilon_f$ ratio. It can be seen that diffusion coefficient is slightly decreasing as the wall/fluid interaction becomes stronger (from hydrophobic to hydrophilic). Since diffusion coefficient is related to fluid atom mobility, we can conclude that a hydrophobic wall in general increases mobility. As we can see D_{ch} is greater near an hydrophobic wall compared to an hydrophilic one. The results are in agreement with the behavior observed in other work (Yen 2013),

On the other hand, we observe that channel shear viscosity presents the inverse behavior compared to diffusion coefficient. Minimum shear viscosity is calculated near the wall for the hydrophobic channels, and it is increasing as wall becomes more hydrophilic. At $\varepsilon_w/\varepsilon_f$ =5.0 is about three times the value for the hydrophobic wall. Shear viscosity is small past an hydrophobic wall, enhancing the flow through the slip-length, which is found larger in this cases, compared to the hydrophilic wall and this result fits well with conclusions obtained from various researchers (Sofos et al. 2013; Cao et al. 2009).

Thermal conductivity does not seem to be affected by wall wettability, as it holds practically its bulk value in all cases investigated. We point out that values calculated using the Green-Kubo formalism by Sofos et al. (2010) fit well in the diagrams in accordance with the general trend observed for the results from the Giannakopoulos et al (2012) method.

Diffusion coefficient calculations in layers across the channel are shown in Fig. 7. For the most hydrophobic channel, the diffusion coefficient increases at the two fluid layers near the wall and is constant, about 15% smaller, in the remaining channel layers. Non-linear behavior across the channel is observed for $\varepsilon_w/\varepsilon_f$ =0.5; small value at layer 1, which slightly increases at layer 2 and stabilizes in the remaining internal fluid layers. The hydrophilic channels ($\varepsilon_w/\varepsilon_f$ =2.0 and 5.0) present very small D_{lay} value at layer1, revealing extremely low fluid mobility, while the internal channel layers reveal increased fluid mobility, greater than the previous hydrophobic channels. It is of interest to point out that wall wettability effect is spread throughout the whole channel region, as diffusion coefficient is concerned, and is not a local parameter affecting only the layer adjacent to the wall.

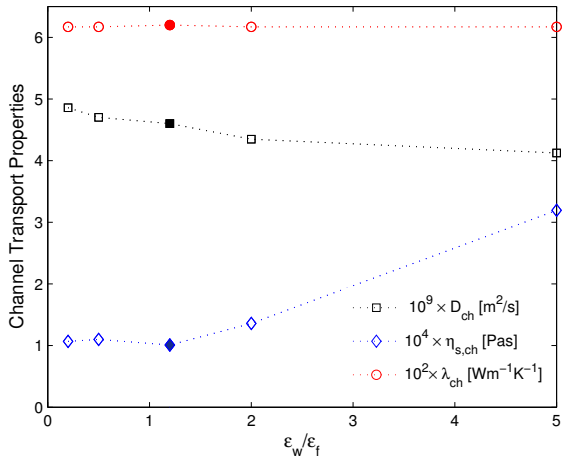

Fig. 6: Channel values for diffusion coefficient, shear viscosity and thermal conductivity versus $\varepsilon_w/\varepsilon_f$ wall wettability ratios. Filled symbols correspond to fully MD-calculated values from (Sofos et al. 2009, 2010). Dotted lines are only a guide to the eye.

Shear viscosity calculation in layers is presented in Fig. 7. At first, we observe that all fluid layers, except layer 1, have similar values across the channel, for every wall/fluid interaction considered in the simulations. Very small values are calculated in layer 1 for $\varepsilon_w/\varepsilon_f$ =5.0, and no effect of the wall is observed for $\varepsilon_w/\varepsilon_f$ =0.2 and 0.5. Values calculated with atomistic NEMD methods for $\varepsilon_w/\varepsilon_f$ =1.2 in Sofos et al. (2010) fit well with the results obtained using the methodology of Giannakopoulos et al. (2012).

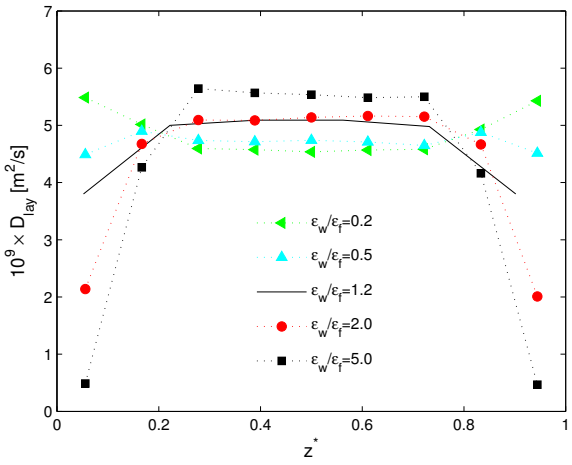

Fig. 7: D_{lay} values for various $\varepsilon_w/\varepsilon_f$ wall wettability ratios, where z^* is the non-dimensional distance normal to the wall, measured from the bottom (lower) wall. Lines are only a guide to the eye.

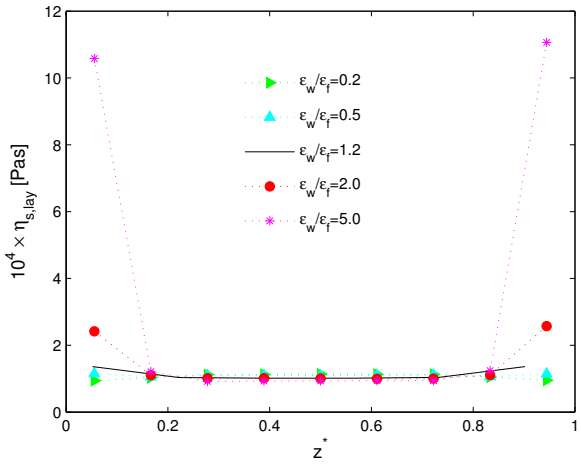

Fig. 8: $\eta_{s,lay}$ values for various $\varepsilon_w/\varepsilon_f$ wall wettability ratios.

Thermal conductivity values along channel layers are practically constant and do not seem to be affected by wall wettability values, as also shown in Fig. 6, so we do not present a diagram here.

It is clear that, although wall wettability is a local characteristic that extends its effect within a small region near the walls, not only does it affect the values of transport properties near the wall, but also their average channel value. Our results also reveal significant effect of wall wettability on flow rates. We consider the volumetric flow rate, i.e., $Q = \bar{v} \cdot A$, where $\bar{v}$ is the average cross-sectional velocity and A is the surface area. Average velocity values for every channel investigated here are shown in Table 1. Since A remains constant, we conclude that flow rate decreases monotonically up to half its value from the most hydrophobic to the hydrophilic channel studied.

Table 1. Average fluid velocity vs. wall wettability

$\varepsilon_w/\varepsilon_f$	0.2	0.5	1.5	2	5
$\bar{v}$ (m/s)	2.4341	2.0176	1.5501	1.4005	1.2344

4. Conclusions

A great range of wall/fluid interaction values are considered in this work, for Molecular Dynamics simulations in nanochannel Poiseuille flows. By means of the radial distribution function, we qualified fluid behavior at the region near the wall channel and found that there is a significant effect of wall wettability in fluid atom ordering. An hydrophilic surface leads in stronger fluid ordering in the fluid layer adjacent to the wall compared to an hydrophobic one.

Diffusion coefficient is found to be affected throughout the whole channel region (for an h=6.3nm channel) from wall wettability, with minimum values for fluid atoms past an hydrophilic wall (about 90% less than the bulk value) and maximum values (about 15% more than the bulk value) in the internal channel layers. Maximum values are also observed in the adjacent to the hydrophobic wall fluid layer.

Flow seems to be enhanced past an hydrophobic wall compared to an hydrophilic one, as shear viscosity behavior reveals.

The effect on diffusion coefficient and shear viscosity can be related to the modification of the fluid structure close to the walls as it is revealed through the radial distribution function.

Thermal conductivity, on the other hand, does not show any variations on our simulations; it remains constant in every simulation case.

Summarizing, in this work it is concluded that

the effect of parameters that are taken into account only at the nanoscale, such as wall hydrophobicity or hydrophilicity, can significantly affect the flow and transport properties and should be incorporated in fundamental theory that drives technological applications in the promising field of nanofluidics and nanotechnology.

Acknowledgement

This project was implemented under the "ARISTEIA II" Action of the "OPERATIONAL PROGRAMME EDUCATION AND LIFELONG LEARNING" and is co-founded by the European Social Fund (ESF) and National Resources.

References

Asproulis, N., D. Drikakis, Phys. Rev. E 81, 061503 (2010).
Baudry J., E. Charlaix, Langmuir 4, 5232 (2001).
Cao, B.Y., J. Sun, M. Chen, Z.Y. Guo, Int. J. Mol. Sci. 10, 4638 (2009).
Giannakopoulos, A.E., F. Sofos, T.E. Karakasidis, A. Liakopoulos, Int. J. Heat Mass Trans. 55, 5087 (2012).
Neto, C., D.R. Evans, E. Bonaccurso, H.-J. Butt, V.S.J. Craig, Rep. Prog. Phys. 68, 2859 (2005).
Sedmik, R.I.P., A.F. Borghesani, K. Heeck, Phys. Fluids 25, 042103 (2013).
Sofos, F., T.E. Karakasidis, A. Liakopoulos. Int. J. Heat Mass Trans. 52, 735 (2009).
Sofos, F., T.E. Karakasidis, A. Liakopoulos. Int. J. Heat Mass Trans. 53, 3839 (2010).
Sofos, F., T.E. Karakasidis, A. Liakopoulos. Microfluid. Nanofluid 12, 25 (2012).
Sofos, F., T.E. Karakasidis, A. Liakopoulos. J. Comp. Theor. Nanosci. 10, 1 (2013).
Tsai, P., A.M. Peters, C. Pirat, M.M Wessling, R.G.H. Lammertink, D. Lohse. Phys. Fluids 21, 112002 (2009).
Vinogradova O.I., A.V. Belyaev, J. Phys: Condens. Matter 23, :184104 (2011)
Priezjev N., A. Darhuber, S. Troian. Phys. Rev. E 71, 041608 (2005).
Voronov, R.S., D.V. Papavassiliou, L.L. Lee, J. Chem. Phys. 124, 204701 (2006).
Yang, S.C., Microfluid. Nanofluid. 2, 501 (2006).
Yen T-H. Microfluid. Nanofluid. doi:10.1007/s10404-013-1299-1. (2013).
Zhang, H., Z. Zhang, H. Ye, Microfluid. Nanofluid. 12, 107 (2012)